International Journal of Geo-Information

MDPI

Article

A New Method Based on Lattice Boltzmann Method and Unsupervised Clustering for Identification of Urban-Scale Ventilation Corridors

Tianyu Li and Peng Xie *

School of Civil Engineering and Geomatics, Shandong University of Technology, Zibo 255000, China; 17663001928@163.com

* Correspondence: xiepenggis@163.com

Abstract: With the increase in urban development intensity, the urban climate has become an important factor affecting sustainable development. The role of urban ventilation corridors in improving urban climate has received widespread attention. Urban ventilation identification and planning based on morphological methods have been initially applied. Traditional morphological methods do not adequately consider the dynamic process of air flow, resulting in a rough evaluation of urban ventilation patterns. This study proposes a new urban-scale ventilation corridor identification method that integrates the Lattice Boltzmann method and the K-means algorithm. Taking Wuhan, China as the research area, an empirical study in different wind directions was conducted on a 20 m grid. The results showed that three levels of ventilation corridors (245.47 km^2 in total) and two levels of ventilation obstruction areas (658.09 km^2 in total) were identified to depict the ventilation pattern of Wuhan's central urban area. The method proposed in this study can meet the needs of urban-scale ventilation corridor identification in terms of spatial coverage, spatial distribution rate and dynamic analysis. Compared with the classic least cumulative ventilation cost method, the method proposed in this study can provide more morphologic details of the ventilation corridors. This plays a very important role in urban planning based on urban ventilation theory.

Keywords: ventilation corridors; ventilation obstruction; urban climate improvement; morphological analysis; Wuhan

Citation: Li, T.; Xie, P. A New Method Based on Lattice Boltzmann Method and Unsupervised Clustering for Identification of Urban-Scale Ventilation Corridors. *ISPRS Int. J. Geo-Inf.* **2024**, *13*, 183. https://doi.org/10.3390/ijgi13060183

Academic Editors: Wolfgang Kainz, Jiangfeng She, Jun Zhu and Min Yang

Received: 9 April 2024
Revised: 27 May 2024
Accepted: 28 May 2024
Published: 31 May 2024

1. Introduction

In recent years, with the acceleration of global urbanization, urban climate issues have gradually become one of the focuses of widespread attention [1–5]. As an important means to mitigate the urban heat island effect, regulate the urban climate, improve air quality and enhance urban livability, urban ventilation corridors have received more and more attention from scholars and urban planners [6–10]. In urban design, understanding the distribution of urban ventilation corridors is of great significance for improving the quality of the urban ecological environment [11–15].

Currently, morphological methods based on geographic information system technology are widely used in urban scale research for urban ventilation analysis. These methods can be classified into three different types: morphological index classification, least cost path (LCP), and circuit theory-based models. A representative morphological index classification method is the Front Area Index (FAI) classification method. This method relies on the correlation between FAI and wind speed. The FAI values are categorized into several different classes by setting thresholds, with lower FAI classes indicating better ventilation. This method is simple to calculate and easy to implement, and is currently the most widely used method [16–20]. However, it is difficult for this method to reflect the differences in urban ventilation patterns under different wind directions and to characterize the impact of upstream ventilation corridors on downstream corridors. The basic idea of the LCP method

is to identify the corridor between the inlet and outlet vents that has the lowest ventilation cost as the main ventilation corridor [21–24]. The LCP method solves the problem of ventilation corridor delineation under different wind directions [24–27]. However, this method can only identify major ventilation corridors, and the identification of the width of the ventilation corridors is a challenging task. The circuit theory-based models assume that when the airflow encounters resistance (represented by morphological indicators), the airflow will be distributed proportionally according to the resistance of each branch. This method is a good solution to identify the width of the ventilation corridors and is very effective in identifying the key nodes in the ventilation corridors [28–31]. However, this method does not fully consider the dynamic process of air flow, resulting in only a rough assessment of urban ventilation corridors.

In order to meet the needs of dynamics, spatial coverage and spatial resolution, the Lattice Boltzmann method (LBM) is used to identify urban ventilation corridors. The LBM can simulate complex fluid processes [32–34]. Running a LBM on an urban space expressed by a morphological index can analyze the spatial distribution of airflow. This method is able to achieve a dynamic analysis of the ventilation pattern under any wind direction. However, the analysis results of the LBM method are continuous values, and it is still difficult to identify the boundaries of the ventilation corridors. Although boundary identification can be performed by setting a series of thresholds, this method is highly subjective. One feasible method is to extract ventilation corridors based on the characteristics of the data itself through machine learning clustering. The K-means clustering algorithm is an effective machine learning algorithm that can perform unsupervised clustering analysis based on the clustering characteristics of the data itself. This helps reduce the impact of subjective factors on the ventilation corridor identification process.

In order to solve the problem of urban ventilation corridor identification, this study integrated the LBM method and the K-means clustering algorithm to propose a framework for automated identification of leveled urban-scale ventilation corridors. This method was then applied to the analysis of the ventilation corridors in Wuhan, China. The realization of the method needs to address the following issues: (1) ventilation patterns under different wind directions, (2) ventilation patterns under seasonal wind frequency weighting, and (3) identification and grading of ventilation corridors and ventilation obstruction zones.

2. Materials and Methods

Based on the building and meteorological data of Wuhan City in 2020, this study combined the LBM model with the K-means clustering algorithm to provide a new way to analyze urban ventilation corridors (Figure 1). The ventilation potential was first calculated by morphological methods. Then, the LBMX model was used to obtain the ventilation distribution pattern in 16 wind directions. Combined with the wind frequency data of the four seasons, a weighted analysis was performed to obtain the ventilation distribution pattern in the four seasons. Finally, the K-means clustering algorithm was applied to obtain graded ventilation corridors and ventilation block areas.

2.1. Basic Structure of LBM

Both space and time are discretized in the LBM. Two-dimensional fluids use a D2Q9 lattice to define the velocity space. There are nine displacement vectors in the lattice, as shown in Figure 2. Among them, the center vector is zero, while the remaining eight vectors point to the eight neighboring cells adjacent to the center cell. The nine displacement vectors are represented by $\vec{e}_i$, where i ranges from zero to eight. Each $\vec{e}_i$ has both x and y components, whose values are -1, 0, or 1, in units of cell spacing Δx.

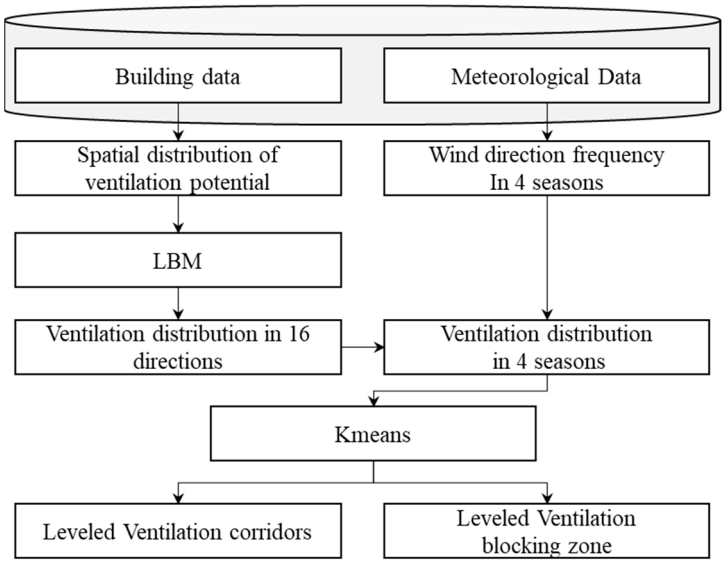

Figure 1. Methodological framework diagram.

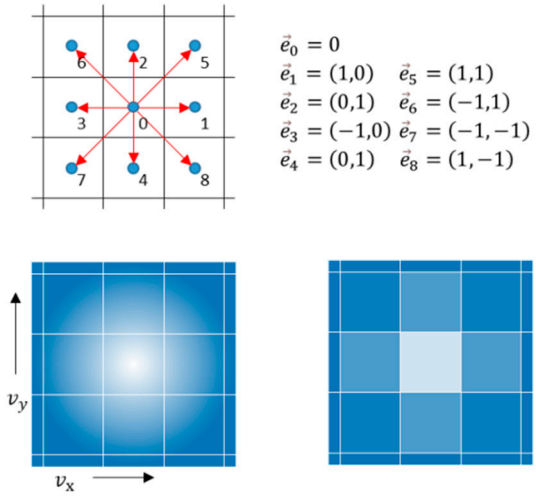

Figure 2. Diagram of the basic LBM model.

2.1.1. Collision Process

LBM involves two basic processes: collision and streaming. In the collision process, the key dynamic variable is the density of the molecule in nine different directions. These nine densities are all positive. Using these density values, it is possible to calculate the total density ρ as well as the components u_x and u_y of the mean velocity in the x and y directions:

$$n_i^{eq} \rho w_i = 1 + 3\vec{e}_i \cdot \vec{u} \left[\frac{9}{2} + \left(\vec{e}_i \cdot \vec{u} \right)^2 - \frac{3}{2} \left| \vec{u} \right|^2 \right] \quad (1)$$

Here w_i represents a set of weights utilized for converting the Boltzmann distribution into a lattice Boltzmann distribution (Figure 1). The relationship between the density in the i direction before the collision (n_i^{old}) and the density in the i direction after the collision (n_i^{new}) can be articulated by the following equation:

$$n_i^{new} = n_i^{old} + \omega \left(n_i^{eq} - n_i^{old} \right) \quad (2)$$

which is the Bhatnagar Gross and Krook model for relaxation to equilibrium via collisions between the molecules of a fluid, where ω is a dimensionless parameter with a value

between 0 and 2. Smaller values of ω mean that the collision time required to reach density equilibrium is longer. On the contrary, a larger value of ω indicates that the collision occurs in a shorter time and thus the equilibrium density is reached more quickly. The value of ω is determined by the viscosity ν of the simulated fluid. This study simulates airflow at room temperature, with T = 25 °C, ν = 0.01834 mPa·s.

$$\nu = \frac{1}{3}\left(\frac{1}{\omega} - \frac{1}{2}\right) \tag{3}$$

2.1.2. Streaming Process

In the streaming process of the LBM model used in this study, as fluid flows between the lattices, a portion can pass from one lattice to an adjacent lattice, while another portion bounces back and stays within its original lattice (Figure 3). The proportion of fluid flowing into a neighboring lattice or being rebounded is related to the ventilation potential of the lattice. The fluid permeability/reflection ratio can be calculated using the following equation:

$$m_j^t = n_j^{t-1} \times o_m + m_i^{t-1} \times (1 - o_n) \tag{4}$$

$$n_i^t = m_i^{t-1} \times o_n + n_j^{t-1} \times (1 - o_m) \tag{5}$$

where m_j^t is the fluid density of the lattice m along the j direction after the t-th iteration of streaming and n_i^t is the fluid density of the lattice n along i the direction after the t-th iteration of streaming. m_i^{t-1} denotes the fluid density of lattice m along the i direction before the t-th iteration of streaming, and n_j^{t-1} denotes the fluid density of lattice n along the j direction before the t-th iteration of streaming. The symbols o_m and o_n denote the fluid ventilation potential of the lattice, respectively.

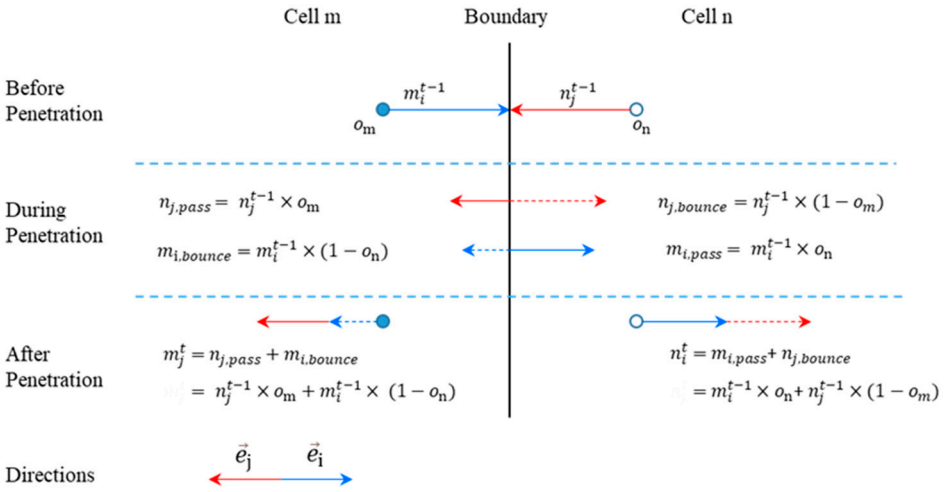

Figure 3. Diagrammatic representation of the infiltration–reflection mechanism.

2.2. Ventilation Potential

FAI is a morphological indicator widely validated and used. It is defined as the ratio of the total windward projected area of a building to the area of the zone. A higher FAI value indicates greater ventilation resistance. The formula is as follows:

$$\lambda_f = \frac{A_f}{A_p} \tag{6}$$

where A_f represents the projected area of the windward side of the building and A_p represents the regional planar area.

The index used in this study indicates the ability of the lattice to allow air to pass through (ventilation potential). Based on FAI, the front ventilation index (FVI) was used to express the ventilation potential (Figure 4). The equation used is as follows:

$$O = \frac{A_h - A_f}{A_p} \tag{7}$$

where A_h represents the total windward projected area with height limit h, A_f is the projected area of the windward side of the building in the same area, and A_p is the planar area of the region. Further, the FVI values were normalized to a range of (0,1).

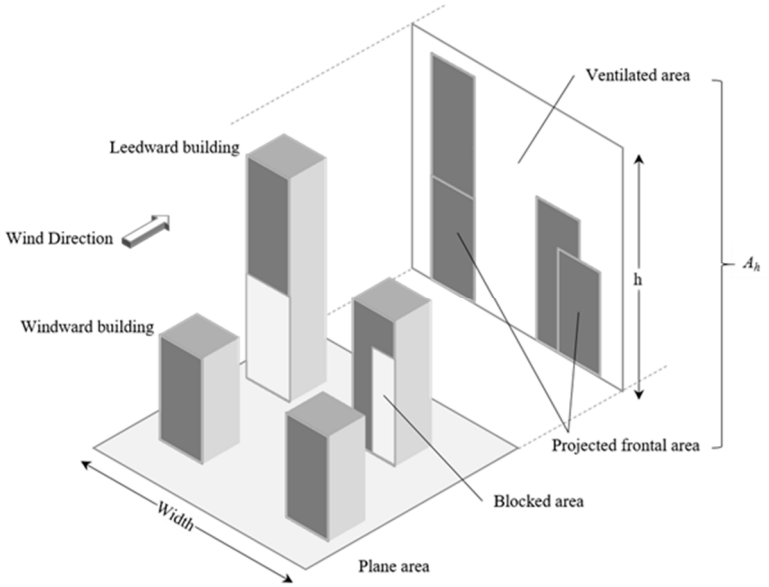

Figure 4. Front ventilation index (FVI) definition.

2.3. K-Means Clustering Algorithm

The K-means algorithm is a clustering algorithm whose goal is to divide a set of data into k different clusters in order to keep the similarity of data within the same cluster high and the similarity between different clusters as low as possible. The basic idea is to randomly select k points as the centers of the clusters, calculate the distance from each data point to the center of the cluster and assign the points to the corresponding clusters. The cluster centers are recalculated and the process is repeated until a stable clustering result is formed.

SSE (sum of squared errors) refers to the sum of the squares of the distances of all of the data points in the clustering result to their corresponding cluster centers. The smaller the value of SSE, the better the clustering effect, which can be used to evaluate the effectiveness of the clustering algorithm. The core idea is to achieve more compact and independent clusters by minimizing the sum of squares of the distances of the data points within a cluster to the cluster center. The stability and convergence of the clusters during the clustering process can be assessed by monitoring the changes in SSE. SSE is an intuitive and effective metric for measuring the performance of K-means clustering. SSE is calculated using the formula:

$$SSE = \sum_{i=1}^{k} \sum_{x \in C_i} (\mu_i - x)^2 \tag{8}$$

where k is the number of clusters, C_i is the i th cluster, and μ_i is the center of the i th cluster.

The Silhouette Coefficient $S(x)$ is an indicator for evaluating the quality of clustering and can be used to judge whether the clustering effect is reasonable or not. The value of the Silhouette Coefficient ranges between $[-1,1]$, and the closer it is to 1, the better the clustering effect. The formula for calculating the Silhouette Coefficient is shown below:

$$S(x) = \frac{b(x) - a(x)}{max(a(x), b(x))} \tag{9}$$

where $a(x)$ denotes the average distance between the data point x and the clustering center to which it belongs, and $b(x)$ denotes the average distance between the data point x and its nearest neighboring clustering center.

2.4. Study Area

Wuhan, the capital of Hubei Province, is an important city in central China (Figure 5). Wuhan has unique geographical conditions, located at the intersection of the Yangtze River and the Han River. Wuhan City comprises three major parts: Hankou (Qiaokou, Jianghan, Jiang'an), Wuchang (Wuchang, Hongshan, Qingshan), and Hanyang. Wuhan has a subtropical monsoon climate, with southerly winds prevailing in summer and northerly winds prevailing in winter. The annual average temperature in Wuhan is 15.8 °C~17.5 °C. The annual precipitation ranges from 1150 mm to 1450 mm. Rainfall is concentrated from June to August every year, accounting for about 40% of the annual rainfall. A mixed forest composed of evergreen broad-leaved forest and deciduous broad-leaved forest is the typical vegetation type in the city. The average altitude of Wuhan's central urban area is 25 m. Wuhan has a long history of urban development and has undergone a rapid expansion of built-up areas in recent years. The problem of urban ventilation has gradually become the main constraint factor for sustainable development in the region. In addition, Wuhan is also one of the earliest cities in China to carry out urban ventilation planning. Taking Wuhan City as the study area, the results of the method proposed in this study can be compared with the results of classic methods, thereby revealing the improvements of the method in this paper. The land use data, roads, administrative divisions, and building data used in this study (as of 2020) were sourced from the Wuhan Urban Planning Bureau, while the meteorological data were sourced from the National Centers for Environmental Information.

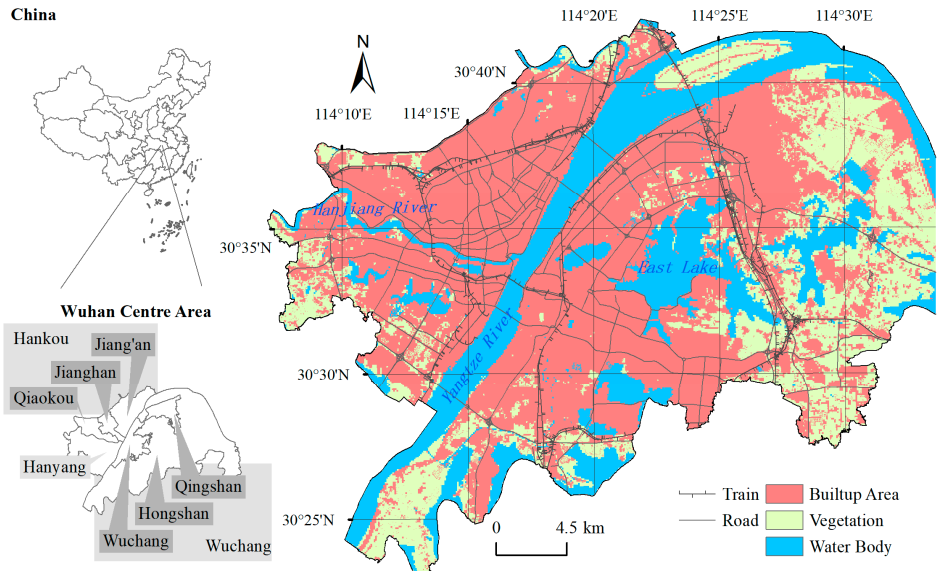

Figure 5. Study area.

3. Results

3.1. Results of the LBMX Multi-Wind Analysis

This study integrated the use of the LBM and K-means methods to carry out the analysis of the ventilation pattern in Wuhan, and the results are shown in Figure 6. The blue area in the figure indicates high ventilation capacity, the orange area indicates low ventilation capacity, and the green area is in between. As a whole, the ventilation capacity spreads from the periphery of the city to the interior, and the intensity gradually decreases. The two middle rivers in the domain, the Yangtze and the Han River, have significantly

better ventilation capacity than the other parts. Secondly, the ventilation capacity of the city suburbs and large lakes spatially connected to the suburbs (e.g., East Lake, Tangxun Lake, etc.) is also high. The areas with low ventilation are mainly located in the urban core of Hankou and Wuchang. The green area indicates a ventilation capacity between the two aforementioned areas and is the most widely distributed in the study area.

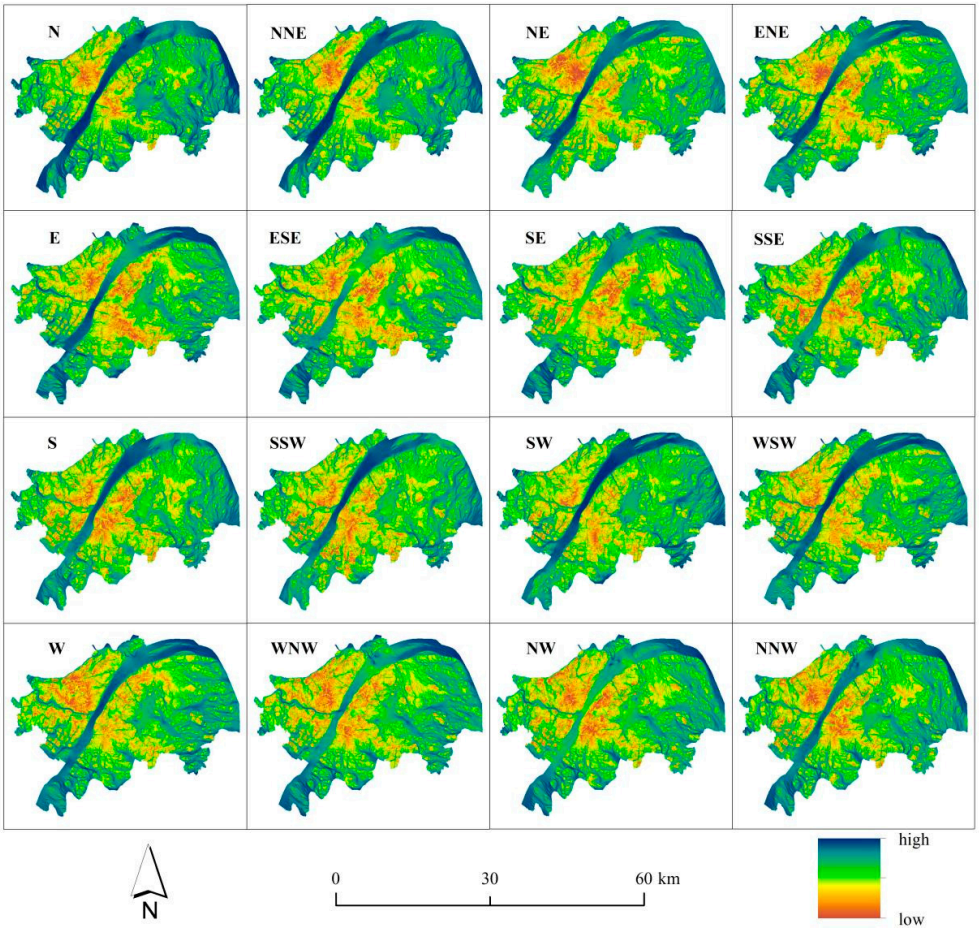

Figure 6. Ventilation distribution in 16 directions.

The urban ventilation pattern varies significantly under different wind directions, and generally shows a spatial pattern consistent with the background wind direction. The Yangtze River shows a northeast–southwest trend in the study area, which is the most important ventilation corridor in the study area. When the background wind direction is northeast–southwest and in a similar wind direction, the ventilation capacity is significantly better than that of the southeast–northwest and similar wind direction scenarios. The Han River is another important natural ventilation corridor in the study area, and its trend and background winds also show similar characteristics. In the suburbs, the spatial trend of the area interspersed by blue and green colors is clearly related to the background wind direction. There is no significant trend in the ventilation corridor shape of East Lake, the largest lake in the study area, but due to different lakeshore shapes, the ventilation capacity above the lake also varies under different winds. Orange and yellow represent areas with poor ventilation capacity, and their spatial distribution patterns are consistent with the background wind direction.

3.2. Wind Frequency Weighted Seasonal Results

In order to reveal whether the ventilation pattern in Wuhan City has obvious seasonal characteristics, based on the frequency of wind directions in each season in Wuhan City, a

weighted overlay analysis was performed on 16 wind direction data to obtain the ventilation distribution pattern of Wuhan City in four seasons. In this study, by integrating the wind data from Tianhe station in 2020, the wind frequency diagrams of the 16 wind directions were produced (Figure 7). From the figure, it can be seen that the overall wind frequency in Wuhan in 2020 is dominated by NNE, followed by NE. The wind direction frequency in the study area has obvious monsoon characteristics. It can be seen from the figure that the wind direction frequencies are similar in spring and summer, while the wind direction frequencies are similar in autumn and winter. The SW and SSW wind directions are significantly more frequent in spring and summer than in autumn and winter, while the NNE and N wind directions are more frequent in autumn and winter than in spring and summer. There is no significant change in the W and E wind directions throughout the year.

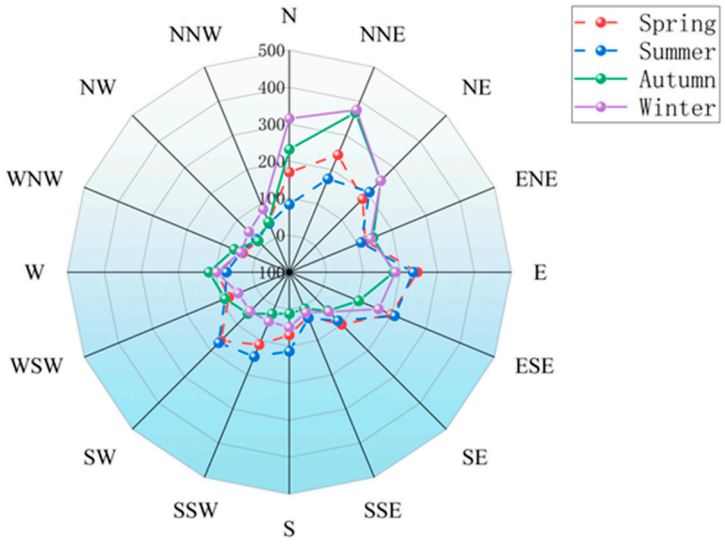

Figure 7. Wind frequency radar map of Wuhan city throughout the year.

Figure 8 shows a distribution map of Wuhan's ventilation pattern in different seasons. The blue, dark green and light green areas in the figure indicate areas with better ventilation, while the orange-red and yellow areas indicate areas with poor ventilation. Overall, blue is mixed with the dark green areas to represent the main ventilation corridors. The light green area shows the distribution area of the capillary ventilation corridors deep inside the city. These capillary ventilation corridors are spread out over a wide area within the city. Orange-red and yellow areas are areas with greater ventilation resistance, mainly distributed in patches within the city.

Figure 9 shows the difference in average ventilation distribution between the four seasons and the whole year. Blue indicates seasonal ventilation is better than the annual average ventilation, while red indicates the opposite. Generally, in spring and summer, ventilation in the Hankou area is better than the annual average, while in Wuchang and Hanyang, they are worse than the annual average. In autumn and winter, the opposite pattern can be found. As Wuhan is wet and cold in winter and hot and humid in summer, this ventilation pattern in Wuchang and Hanyang aggravates physical discomfort. Specifically, in spring, Hankou presents a continuous blue area, a striped blue distribution appears on the south side of Wuchang, and a large red area appears in the central area of Wuchang. In summer, the intensity of the blue area in Hankou area weakens but is still distributed continuously. The striped blue area south of Wuchang weakens significantly and the red area moves southward. The patterns in autumn and winter are similar, with Hankou showing obvious red areas, while Wuchang and Hanyang mostly show blue or yellow areas mixed with band-shaped red areas.

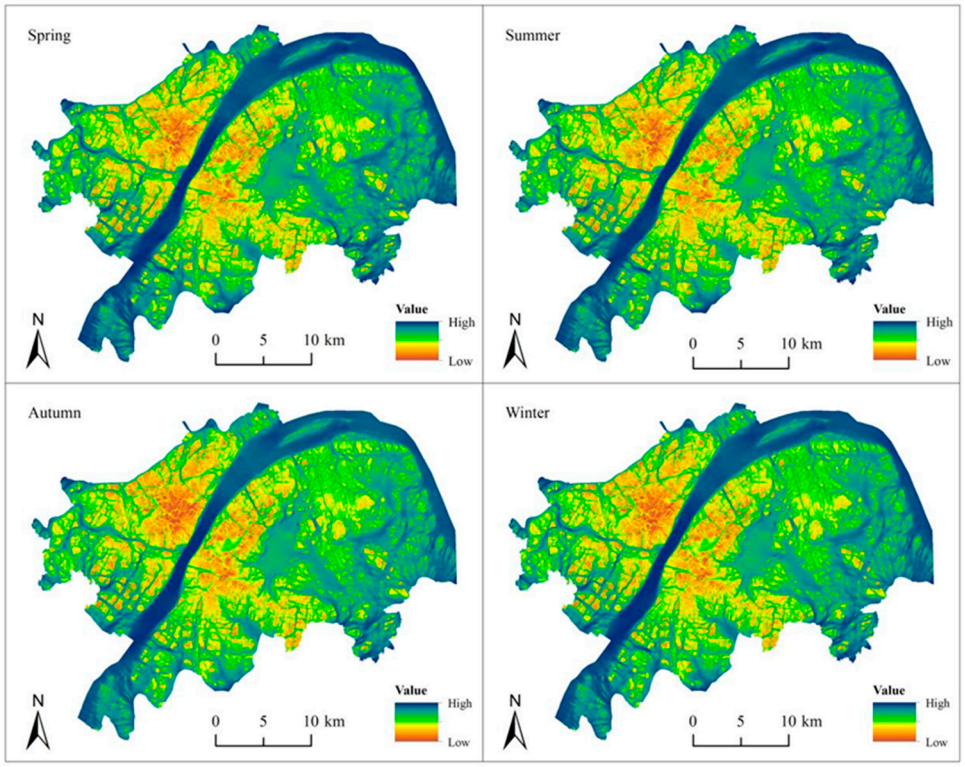

Figure 8. Distribution of ventilation patterns by season.

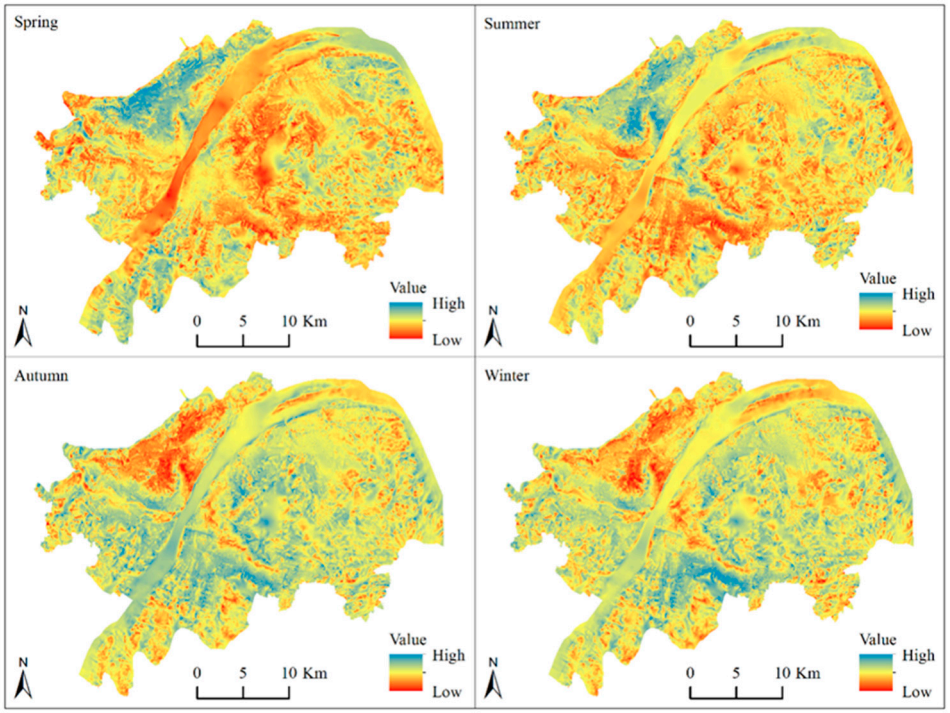

Figure 9. Difference in ventilation distribution between the four seasons and the annual average.

3.3. Ventilation Corridors and Ventilation Obstruction

The ventilation distribution pattern in Wuhan City has a high consistency among seasons. In this study, the K-means clustering method was applied to aggregate the annual ventilation distribution in Wuhan, and five categories were formed. Three of the categories

are ventilation corridors (Figure 10), and two categories are ventilation obstruction areas (Figure 11).

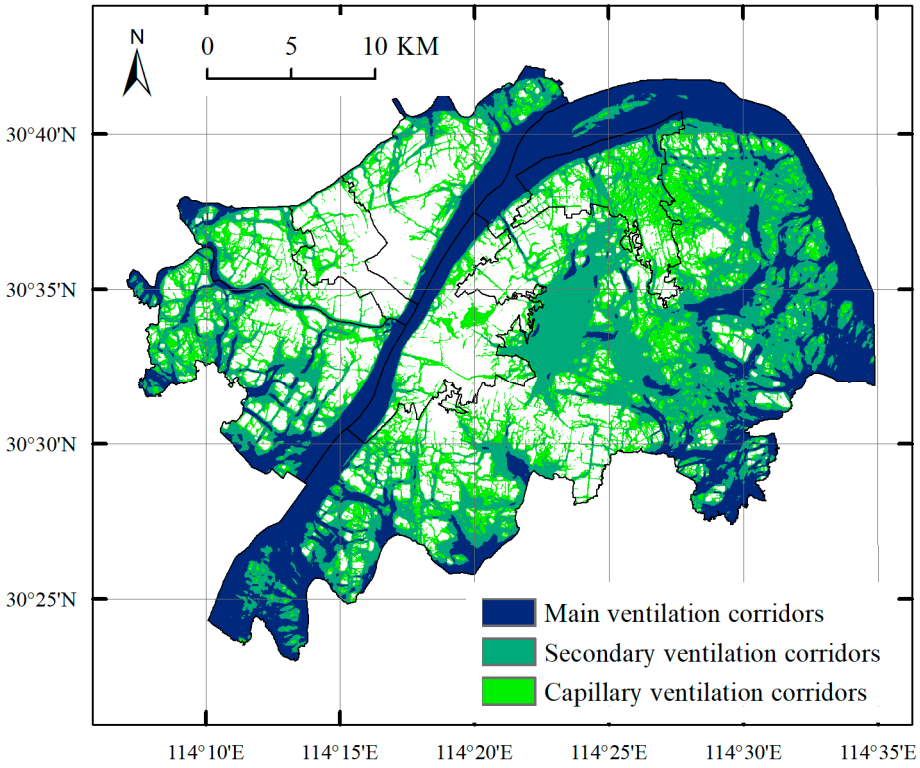

Figure 10. Map of classified ventilation corridor.

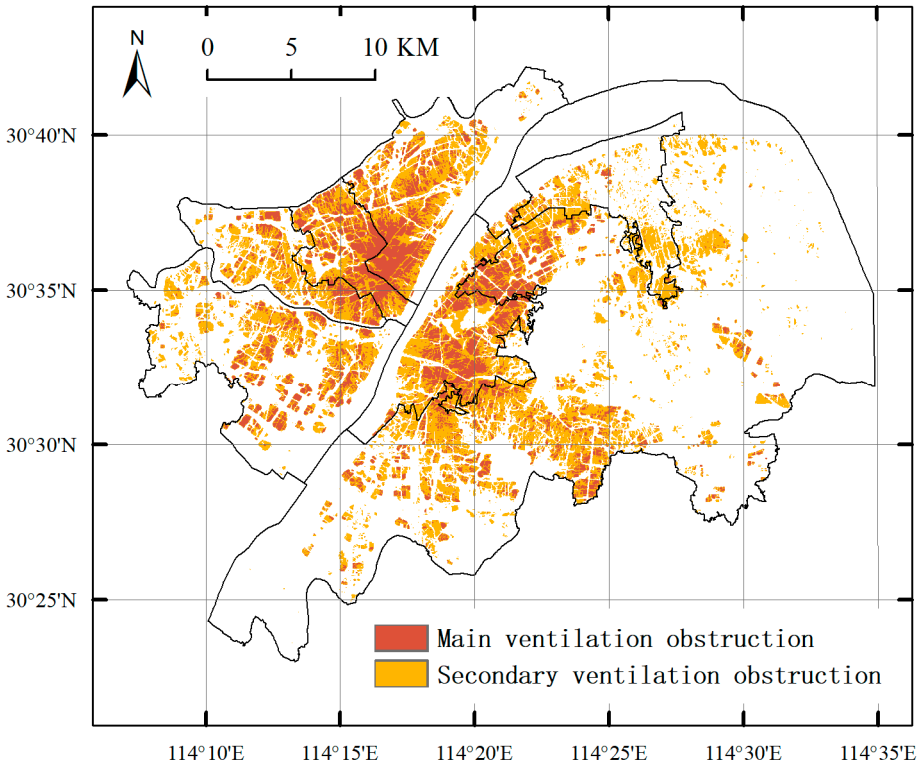

Figure 11. Map of ventilation obstruction areas.

As shown in Figure 10, the blue, dark green and light green zones represent main ventilation corridors, secondary ventilation corridors and capillary ventilation corridors, respectively. The blue zone (234.38 km^2), as the main ventilation corridor of the city, is decisive for the formation of the overall ventilation pattern of the city. Large water bodies such as the Yangtze River, Han River, South Lake, and Tangxun Lake have vast open spaces. These natural ventilation corridors are located between the city center and the suburbs, allowing air to be quickly exchanged between areas, creating an ideal ventilation environment in the city.

The dark green areas (252.80 km^2), as secondary ventilation corridors within the city, are slightly less effective than the blue areas, but they still play a positive role in improving the urban environment. Secondary ventilation corridors are the spatial continuation of the main ventilation corridors. The main ventilation corridors influence and rely on them to extend further into the city. From the figure, it can be found that large dark green areas are distributed around large lakes such as Nanhu Lake, Yanxi Lake, and Tangxun Lake.

The light green areas (170.91 km^2), as capillary ventilation corridors, are spread throughout the city. The capillary ventilation corridors are widely distributed and mainly consist of small lakes, small rivers, and roads. Their distinctive feature is that their spatial distribution is narrower and fragmented.

As shown in Figure 11, the distribution of ventilation obstruction areas in Wuhan is shown with an orange color. These areas are affected by upstream and downstream airflow and their own ventilation potential, resulting in relatively poor ventilation effects. Spatially, such areas are mainly distributed in dense urban high-rise residential areas and commercial areas. Among them, the area between Jiang'an District and Jianghan District on the north side of the Yangtze River, and the area around Shahu Lake on the south side of the Yangtze River, have the worst ventilation. These areas are urban core areas with a dense population, high land prices, and high development intensity. The buildings are mainly commercial buildings and high-rise residential buildings, resulting in the worst ventilation effect in this area. Although there are many small open spaces in this area, they are not spatially continuous and do not form significant ventilation corridors.

Yellow areas (168.67 km^2), are relatively better ventilated than orange areas (76.80 km^2). Spatially, such areas are distributed around the orange area, mainly in Qingshan District, the north and south of Hongshan District, and the east of Hanyang District. Although these areas are close to the urban core, their connection to the city's outskirts gives them potential ventilation capabilities. There are still a large number of low-rise old apartment buildings in these areas, which are expected to become key planning areas to improve urban ventilation effects.

3.4. Comparison of Different Methods

Figure 12 shows the Wuhan ventilation corridors planning map, the results based on the least cumulative ventilation cost method [35], and the results of the proposed method. It can be seen from the figure that the results of the two ventilation corridor identification methods are highly consistent with the current ventilation planning. Furthermore, compared with the least cumulative ventilation cost method (working on a 100 m grid), the method proposed in this study (working on a 20 m grid) can provide more details of the ventilation corridor morphology. Based on the morphological details of the ventilation corridors, further detailed adjustments to the urban architectural form can be made. This is of great significance for improving the ventilation environment in an already highly developed urban area.

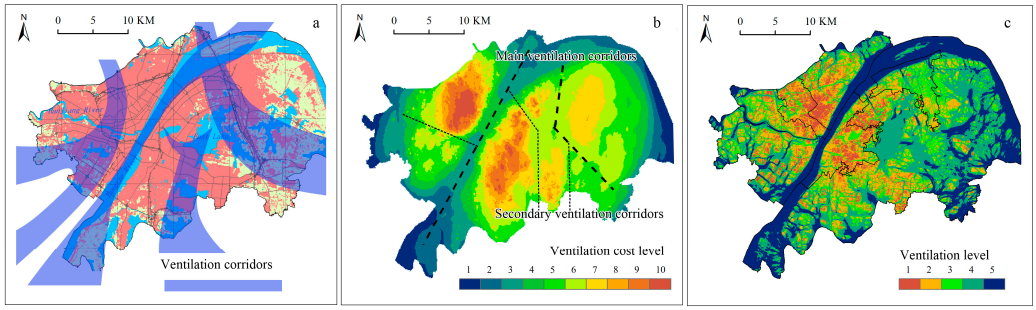

Figure 12. Maps of ventilation from different methods: (**a**) the Wuhan ventilation corridors planning map (modified), (**b**) ventilation cost level analyzed by the classic least cumulative ventilation cost method, (**c**) ventilation level analyzed by the proposed method.

4. Discussion

4.1. Advantages

Identifying ventilation corridors at the urban scale is an issue of widespread concern. Classic methods such as the morphological index classification method, the least cost path method and the method based on circuit theory have been proposed successively. However, these methods all have shortcomings in results coverage, spatial resolution and dynamic analysis capabilities. The LBM method overcomes the limitations of traditional methods in spatial resolution and improves the ability to analyze the details of the ventilation corridors but has difficulties in achieving hierarchical classification of the ventilation corridors. This study used a combination of the LBM method and K-means clustering algorithm to solve the above problems. The method proposed in this article can objectively identify ventilation corridors with grade information, thereby avoiding subjective interference in the corridor identification process. In addition, ventilation-obstructed areas were identified in this study.

4.2. Ventilation Patterns in Wuhan

This study identified three levels of ventilation corridors in Wuhan:

(1). Major ventilation corridors, such as the Yangtze River and Han River, as well as large lakes and open areas around the city;

(2). Secondary ventilation corridors, such as main urban arteries and natural open spaces within the city;

(3). Capillary ventilation corridors, which are widely distributed around secondary ventilation corridors and are mainly composed of urban streets.

Regarding Wuhan's ventilation layout, attention needs to be paid to protecting and utilizing the rich lake resources in the region. First, there is a need to actively protect the regional lakes and various types of open spaces to avoid encroachment on construction land. Secondly, when developing buildings near lakes and open spaces, sufficient space should be reserved in the direction of high-frequency winds so that ventilation corridors can be formed to avoid the occurrence of sand lake cases.

This study extracted two levels of ventilation obstruction areas in Wuhan: the red area has the worst ventilation conditions. These areas are the economically developed business districts of Wuhan, with dense population, and the buildings are mainly commercial buildings and high-rise residential buildings. For this area, urban development density should be strictly limited and further strengthened. Secondly, during the process of demolishing the old and building new ones, open space should be ensured and its connectivity layout should be strengthened. It is difficult to improve ventilation in these areas, so priority should be given to using building materials, vertical greening and other methods to improve the urban climate. Yellow areas have slightly better ventilation than red areas, and these areas have relatively lower building heights and densities. These areas are closer to the main ventilation corridors and exhibit the characteristics of fragmented distributions in space. Taking these characteristics into account, the yellow areas are expected to become key planning areas to improve urban ventilation effects.

4.3. Limitations

The method proposed in this study still has limitations. Due to limitations of computing power, this study only conducted empirical analysis on the central urban area of Wuhan. The impact of buildings outside the central urban area on ventilation corridors in Wuhan has not been analyzed. A potential solution to this problem is parallel computing to improve the efficiency of the method. This can not only expand the research area to the surrounding areas of the city, but also further improve the spatial resolution of the analysis results. In addition, since different cities have different climate characteristics, in actual planning applications, wind speed sampling data should also be combined to optimize the number and thresholds of ventilation corridors and ventilation obstruction area levels.

5. Conclusions

This study proposes an urban-scale ventilation corridor analysis method that integrates LBM and K-means algorithms. Taking the central urban area of Wuhan as the research area, the ventilation layout of 16 wind directions was analyzed. The seasonal differences in ventilation patterns were analyzed based on the frequency of wind directions in the four seasons. The K-means clustering algorithm was used to identify ventilation corridors and ventilation block areas. The results showed that (1) this method can meet the requirements of ventilation corridor analysis in terms of spatial coverage, spatial resolution, dynamic wind direction and corridor grade identification. (2) The spatial pattern of three levels of ventilation corridors (245.47 km^2 in total) and two levels of ventilation obstruction areas (658.09 km^2 in total) can describe the ventilation pattern of Wuhan City. (3) Compared with the classic method, the method proposed in this study can provide more analysis of the spatial form of ventilation corridors, which plays an important role in detailed urban form planning.

However, this study still has some shortcomings. For example, due to limitations in computing power, only the central urban area was analyzed. This problem can be solved by introducing parallel computing methods. In addition, the three levels of ventilation corridors and the two levels of ventilation obstruction areas applied in this study are just a case to demonstrate how to use the proposed method. In real planning applications, the actual wind speed sampling data in the study area should be integrated to optimize the number and thresholds of levels of ventilation corridors and obstruction areas.

Author Contributions: Conceptualization, Peng Xie and Tianyu Li; methodology, Peng Xie and Tianyu Li; software, Peng Xie; validation, Peng Xie and Tianyu Li; formal analysis, Peng Xie and Tianyu Li; investigation, Peng Xie and Tianyu Li; resources, Peng Xie and Tianyu Li; data curation, Peng Xie and Tianyu Li; writing—original draft preparation, Peng Xie and Tianyu Li; writing—review and editing, Peng Xie; visualization, Peng Xie and Tianyu Li; supervision, Peng Xie; project administration, Peng Xie; funding acquisition, Peng Xie. All authors have read and agreed to the published version of the manuscript.

Funding: This research was funded by the National Natural Science Foundation of China Youth Program, grant number 42201466, and the Shandong Province Natural Science Foundation Youth Branch, grant number ZR2021QD078.

Data Availability Statement: The raw data supporting the conclusions of this article will be made available by the authors on request.

Conflicts of Interest: The authors declare no conflicts of interest.

References

1. He, B.-J.; Ding, L.; Prasad, D. Wind-Sensitive Urban Planning and Design: Precinct Ventilation Performance and Its Potential for Local Warming Mitigation in an Open Midrise Gridiron Precinct. *J. Build. Eng.* **2020**, *29*, 101145. [CrossRef]
2. Qiao, Z.; Wang, N.; Chen, J.; He, T.; Xu, X.; Liu, L.; Sun, Z.; Han, D. Urbanization Accelerates Urban Warming by Changing Wind Speed: Evidence from China Based on 2421 Meteorological Stations from 1978 to 2017. *Environ. Impact Assess. Rev.* **2023**, *102*, 107189. [CrossRef]

3. Aslam, B.; Maqsoom, A.; Khalid, N.; Ullah, F.; Sepasgozar, S. Urban Overheating Assessment through Prediction of Surface Temperatures: A Case Study of Karachi, Pakistan. *ISPRS Int. J. Geo-Inf.* **2021**, *10*, 539. [CrossRef]
4. Ku, C.-A.; Tsai, H.-K. Evaluating the Influence of Urban Morphology on Urban Wind Environment Based on Computational Fluid Dynamics Simulation. *ISPRS Int. J. Geo-Inf.* **2020**, *9*, 399. [CrossRef]
5. Deininger, M.E.; Von Der Grün, M.; Piepereit, R.; Schneider, S.; Santhanavanich, T.; Coors, V.; Voß, U. A Continuous, Semi-Automated Workflow: From 3D City Models with Geometric Optimization and CFD Simulations to Visualization of Wind in an Urban Environment. *ISPRS Int. J. Geo-Inf.* **2020**, *9*, 657. [CrossRef]
6. Gong, D.; Dai, X.; Zhou, L. Satellite-Based Optimization and Planning of Urban Ventilation Corridors for a Healthy Microclimate Environment. *Sustainability* **2023**, *15*, 15653. [CrossRef]
7. Palusci, O.; Cecere, C. Urban Ventilation in the Compact City: A Critical Review and a Multidisciplinary Methodology for Improving Sustainability and Resilience in Urban Areas. *Sustainability* **2022**, *14*, 3948. [CrossRef]
8. Shen, X.; Liu, H.; Yang, X.; Zhou, X.; An, J.; Yan, D. A Data-Mining-Based Novel Approach to Analyze the Impact of the Characteristics of Urban Ventilation Corridors on Cooling Effect. *Buildings* **2024**, *14*, 348. [CrossRef]
9. Xu, W.; Zhao, L.; Zhang, Y.; Gu, Z. Investigation on Air Ventilation within Idealised Urban Wind Corridors and the Influence of Structural Factors with Numerical Simulations. *Sustainability* **2023**, *15*, 13817. [CrossRef]
10. Zeng, L.; Zhang, X.; Lu, J.; Li, Y.; Hang, J.; Hua, J.; Zhao, B.; Ling, H. Influence of Various Urban Morphological Parameters on Urban Canopy Ventilation: A Parametric Numerical Study. *Atmosphere* **2024**, *15*, 352. [CrossRef]
11. He, B.-J.; Ding, L.; Prasad, D. Relationships among Local-Scale Urban Morphology, Urban Ventilation, Urban Heat Island and Outdoor Thermal Comfort under Sea Breeze Influence. *Sustain. Cities Soc.* **2020**, *60*, 102289. [CrossRef]
12. He, B.-J.; Ding, L.; Prasad, D. Urban Ventilation and Its Potential for Local Warming Mitigation: A Field Experiment in an Open Low-Rise Gridiron Precinct. *Sustain. Cities Soc.* **2020**, *55*, 102028. [CrossRef]
13. Qiao, Z.; Xu, X.; Wu, F.; Luo, W.; Wang, F.; Liu, L.; Sun, Z. Urban Ventilation Network Model: A Case Study of the Core Zone of Capital Function in Beijing Metropolitan Area. *J. Clean. Prod.* **2017**, *168*, 526–535. [CrossRef]
14. Chen, C.; Ye, S.; Bai, Z.; Wang, J.; Nedzved, A.; Ablameyko, S. Intelligent Mining of Urban Ventilated Corridor Based on Digital Surface Model under the Guidance of K-Means. *ISPRS Int. J. Geo-Inf.* **2022**, *11*, 216. [CrossRef]
15. Zhou, L.; Ma, L.; Johnson, B.A.; Yan, Z.; Li, F.; Li, M. Patch-Based Local Climate Zones Mapping and Population Distribution Pattern in Provincial Capital Cities of China. *ISPRS Int. J. Geo-Inf.* **2022**, *11*, 420. [CrossRef]
16. Gál, T.; Unger, J. Detection of Ventilation Paths Using High-Resolution Roughness Parameter Mapping in a Large Urban Area. *Build. Environ.* **2009**, *44*, 198–206. [CrossRef]
17. Suder, A.; Szymanowski, M. Determination of Ventilation Channels In Urban Area: A Case Study of Wrocław (Poland). *Pure Appl. Geophys.* **2014**, *171*, 965–975. [CrossRef]
18. Wicht, M.; Wicht, A.; Osińska-Skotak, K. Detection of Ventilation Corridors Using a Spatio-Temporal Approach Aided by Remote Sensing Data. *Eur. J. Remote Sens.* **2017**, *50*, 254–267. [CrossRef]
19. Xu, F.; Gao, Z. Frontal Area Index: A Review of Calculation Methods and Application in the Urban Environment. *Build. Environ.* **2022**, *224*, 109588. [CrossRef]
20. Yuan, C.; Ren, C.; Ng, E. GIS-Based Surface Roughness Evaluation in the Urban Planning System to Improve the Wind Environment—A Study in Wuhan, China. *Urban Clim.* **2014**, *10*, 585–593. [CrossRef]
21. Hsieh, C.-M.; Huang, H.-C. Mitigating Urban Heat Islands: A Method to Identify Potential Wind Corridor for Cooling and Ventilation. *Comput. Environ. Urban Syst.* **2016**, *57*, 130–143. [CrossRef]
22. Ling Chen, S.; Lu, J.; Yu, W.W. A Quantitative Method to Detect the Ventilation Paths in a Mountainous Urban City for Urban Planning: A Case Study in Guizhou, China. *Indoor Built Environ.* **2017**, *26*, 422–437. [CrossRef]
23. Wong, M.S.; Nichol, J.E.; To, P.H.; Wang, J. A Simple Method for Designation of Urban Ventilation Corridors and Its Application to Urban Heat Island Analysis. *Build. Environ.* **2010**, *45*, 1880–1889. [CrossRef]
24. Fang, Y.; Gu, K.; Qian, Z.; Sun, Z.; Wang, Y.; Wang, A. Performance Evaluation on Multi-Scenario Urban Ventilation Corridors Based on Least Cost Path. *J. Urban Manag.* **2021**, *10*, 3–15. [CrossRef]
25. Li, Q.; Zheng, J.; Yuan, S.; Zhang, L.; Dong, R.; Fu, H. RAV Model: Study on Urban Refined Climate Environment Assessment and Ventilation Corridors Construction. *Build. Environ.* **2024**, *248*, 111080. [CrossRef]
26. Liu, X.; Huang, B.; Li, R.; Zhang, J.; Gou, Q.; Zhou, T.; Huang, Z. Wind Environment Assessment and Planning of Urban Natural Ventilation Corridors Using GIS: Shenzhen as a Case Study. *Urban Clim.* **2022**, *42*, 101091. [CrossRef]
27. Shi, Z.; Yang, J.; Zhang, Y.; Xiao, X.; Xia, J.C. Urban Ventilation Corridors and Spatiotemporal Divergence Patterns of Urban Heat Island Intensity: A Local Climate Zone Perspective. *Environ. Sci. Pollut. Res.* **2022**, *29*, 74394–74406. [CrossRef] [PubMed]
28. Qian, W.; Li, X. A Cold Island Connectivity and Network Perspective to Mitigate the Urban Heat Island Effect. *Sustain. Cities Soc.* **2023**, *94*, 104525. [CrossRef]
29. Xie, P.; Yang, J.; Wang, H.; Liu, Y.; Liu, Y. A New Method of Simulating Urban Ventilation Corridors Using Circuit Theory. *Sustain. Cities Soc.* **2020**, *59*, 102162. [CrossRef]
30. Xie, P.; Yang, J.; Sun, W.; Xiao, X.; Cecilia Xia, J. Urban Scale Ventilation Analysis Based on Neighborhood Normalized Current Model. *Sustain. Cities Soc.* **2022**, *80*, 103746. [CrossRef]
31. Yu, Z.; Zhang, J.; Yang, G. How to Build a Heat Network to Alleviate Surface Heat Island Effect? *Sustain. Cities Soc.* **2021**, *74*, 103135. [CrossRef]

32. Ahmad, N.H.; Inagaki, A.; Kanda, M.; Onodera, N.; Aoki, T. Large-Eddy Simulation of the Gust Index in an Urban Area Using the Lattice Boltzmann Method. *Bound.-Layer Meteorol.* **2017**, *163*, 447–467. [CrossRef]
33. King, M.-F.; Khan, A.; Delbosc, N.; Gough, H.L.; Halios, C.; Barlow, J.F.; Noakes, C.J. Modelling Urban Airflow and Natural Ventilation Using a GPU-Based Lattice-Boltzmann Method. *Build. Environ.* **2017**, *125*, 273–284. [CrossRef]
34. Obrecht, C.; Kuznik, F.; Merlier, L.; Roux, J.-J.; Tourancheau, B. Towards Aeraulic Simulations at Urban Scale Using the Lattice Boltzmann Method. *Environ. Fluid Mech.* **2015**, *15*, 753–770. [CrossRef]
35. Xie, P.; Liu, D.; Liu, Y.; Liu, Y. A Least Cumulative Ventilation Cost Method for Urban Ventilation Environment Analysis. *Complexity* **2020**, *2020*, 1–13. [CrossRef]